Journal of Power Sources 228 (2013) 270–280

Contents lists available at SciVerse ScienceDirect

Journal of Power Sources

journal homepage: www.elsevier.com/locate/jpowsour

High performance silicon free-standing anodes fabricated by low-pressure and plasma-enhanced chemical vapor deposition onto carbon nanotube electrodes

Michael W. Forney [a], Roberta A. DiLeo [a], Alan Raisanen [a,c], Matthew J. Ganter [a], Jason W. Staub [a], Reginald E. Rogers [a,b], Richard D. Ridgley [d], Brian J. Landi [a,b,*]

[a] NanoPower Research Laboratories, Rochester Institute of Technology, Rochester, NY 14623, USA
[b] Chemical & Biomedical Engineering, Rochester Institute of Technology, 160 Lomb Memorial Drive, Rochester, NY 14623, USA
[c] Manufacturing and Mechanical Engineering Technology/Packaging Science, Rochester Institute of Technology, Rochester, NY 14623, USA
[d] US Government, Washington DC, USA

HIGHLIGHTS

- Silicon–carbon nanotube anodes fabricated by two chemical vapor deposition methods.
- Electrochemical performance studied as function of silicon loading for both methods.
- Anode capacities of 2500 mAh g^{-1} and Si-only capacities of 3780 mAh g^{-1} measured.
- Anode morphology and performance depends on chemical vapor deposition method.
- Postmortem analysis shows significant differences in anode morphology after cycling.

ARTICLE INFO

Article history:
Received 24 August 2012
Received in revised form
16 November 2012
Accepted 22 November 2012
Available online 1 December 2012

Keywords:
Lithium ion battery
Low pressure chemical vapor deposition
Plasma enhanced chemical vapor deposition
Silicon
Anode
Carbon nanotube

ABSTRACT

High capacity silicon and alternative current collectors are being evaluated as a viable approach to increase the energy density of lithium ion batteries. Presently, silicon is deposited onto lightweight single-walled carbon nanotube (SWCNT) current collectors by low-pressure chemical vapor deposition (LPCVD) and plasma-enhanced chemical vapor deposition (PECVD) to form Si-SWCNT free-standing anodes. The electrode morphology is characterized by scanning electron microscopy (SEM) and Raman spectroscopy, and the electrochemical performance is studied for each CVD method at silicon weight loadings between 25% and 70%. Results demonstrate that PECVD fabricated Si-SWCNT anodes outperform LPCVD fabricated anodes, with electrode extraction capacities as high as 2500 mAh g^{-1}. When only the Si mass is considered, PECVD-Si-SWCNT anodes have up to 2x higher extraction capacities than LPCVD-Si-SWCNT anodes at low Si loadings. The highest Si-only extraction capacity measured was 3780 mAh g^{-1}. Full cells were demonstrated to have stable cycling for 100 cycles. Postmortem analysis (via SEM and Raman) reveals that PECVD-Si-SWCNT anodes undergo more significant morphological and crystallographic changes during cycling than LPCVD-Si-SWCNT anodes. This work demonstrates that the choice of CVD method for Si deposition onto SWCNT current collectors greatly impacts the resulting electrode morphology, which, in turn, affects the electrochemical performance.

1. Introduction

Lithium ion batteries have emerged as a leading energy storage technology for many mobile applications, such as portable electronics, electric vehicles, and renewable energy storage, due to their high energy density and minimal self-discharge [1,2]. The prospect to increase energy density relies upon approaches to synthesize electrodes from high capacity active materials and alternative electrode designs. The semiconductor materials germanium and silicon are promising anode active materials that have theoretical capacities of 1600 mAh g^{-1} [3] and 4200 mAh g^{-1} [4], respectively. By substituting these high capacity materials for conventional graphitic active materials, gains in electrode energy density can be achieved due to active mass reduction. Moreover, elimination of inactive mass from the electrode is just as essential for further

* Corresponding author. Chemical & Biomedical Engineering, Rochester Institute of Technology, 160 Lomb Memorial Drive, Rochester, NY 14623, USA. Tel.: +1 585 475 4726; fax: +1 585 475 7890.
E-mail addresses: bjlsps@rit.edu, brian.landi@rit.edu (B.J. Landi).

0378-7753/$ – see front matter © 2012 Elsevier B.V. All rights reserved.
http://dx.doi.org/10.1016/j.jpowsour.2012.11.109

increases in energy density, especially the copper foil current collector [5,6]. One approach for replacing copper is to use highly conductive carbon nanotubes (CNTs) to reduce the current collector mass by an order of magnitude [2,7]. Other potential benefits of replacing copper with CNTs include increased depth of discharge (copper oxidizes below 2.5 V), storage at near-zero volt state of charge, and high temperature applications (>200 °C) [2]. Combination of these two approaches (high capacity active materials and alternative current collectors) provides the greatest opportunity for developing anodes with the highest possible capacities.

Silicon is being investigated as nanoparticles, nanowires, and thin films to help mitigate the capacity fade from volume changes that occur during lithium insertion/extraction, leading to pulverization [3,4]. CNTs have also been studied for lithium storage as free-standing electrodes with capacities greater than MCMBs [8]. Several methods for combining silicon (Si) and CNTs have been published in the literature [9–14]. One approach is to ball mill Si powder and multi-walled CNTs (MWCNTs) or single-walled CNTs (SWCNTs) to form Si-CNT composites, with binder, that can be coated onto a copper foil current collector [9,10]. The CNTs help form an electrical percolation network between the Si particles [10] and the electrochemical performance of the active material is good, but this method still requires the use of a copper foil current collector. A second approach is to attach Si nanoparticles (NPs) to CNTs, either by covalent linkage [11] or silane low-pressure chemical vapor deposition (LPCVD) [12–14]. Similar to the first approach, these active materials were supported on copper foil. A more disruptive approach requires replacing the copper current collector with an alternative lightweight current collector, as recently demonstrated for Ge-thin films [5]. It has been demonstrated that free-standing (i.e., no copper) Si-CNT electrodes can be fabricated using LPCVD to coat CNT networks that serve as the current collector [14,15], showing that CVD deposition of Si onto CNT networks is a viable approach to ultra high capacity anodes. An alternative CVD technique is plasma-enhanced CVD (PECVD), which has potential for scale-up, as it has been used for industrial roll-to-roll deposition of amorphous Si for solar cell applications [16]. Therefore, a systematic study is needed to compare the performance of Si-CNT anodes fabricated by these prevalent CVD techniques.

In this paper, silicon is deposited onto free-standing SWCNT current collectors by LPCVD and PECVD, without the use of a binder or a copper current collector. The surface morphology and crystallinity of as-deposited Si films are compared by scanning electron microscopy (SEM) and Raman spectroscopy, respectively. The Si-SWCNT electrodes are tested electrochemically vs. lithium to determine which method of Si deposition yields higher coulombic efficiency and higher extraction capacity. Cycling performance is tested by pairing Si-CNT anodes with $LiNi_{0.8}Co_{0.1}Al_{0.1}O_2$ (NCA) cathodes. Lastly, the morphology and crystallinity of the Si-SWCNT electrodes is characterized by postmortem SEM and Raman to understand changes that occur during the initial cycles.

2. Experimental

2.1. Electrode preparation

Single-walled carbon nanotubes (SWCNTs) were synthesized by laser vaporization and purified, as described in previous work [17,18]. SWCNT current collectors were fabricated [8] with areal densities of ~1 mg cm^{-2} (see Fig. 1a/b). The areal density of SWCNT current collectors was determined by measuring the mass of the SWCNT paper on a microbalance (Mettler Toledo XP2U Ultra-microbalance) and measuring the area of the SWCNT paper using ImageJ [19] for image analysis. After Si deposition, the areal density was re-measured using the same technique to determine the areal density of Si deposited.

Low pressure chemical vapor deposition (LPCVD) of silicon was performed with an ASM 6" LPCVD (see schematic in Fig. 1c). The operating temperature was 500 °C and the operating pressure was 1 Torr. Pure silane gas flow was 50 sccm, and deposition times were typically between 10 and 60 min. Samples were masked to preferentially deposit Si on one side of the SWCNT paper. Si-SWCNT samples fabricated by LPCVD show excellent mechanical stability, and can be bent repeatedly like a piece of paper, which is consistent with recently published work on a similar Si-CNT system [20].

Plasma-enhanced chemical vapor deposition (PECVD) of silicon was performed with an AME P5000 PECVD (see schematic in Fig. 1d). The operating temperature was 400 °C and the operating

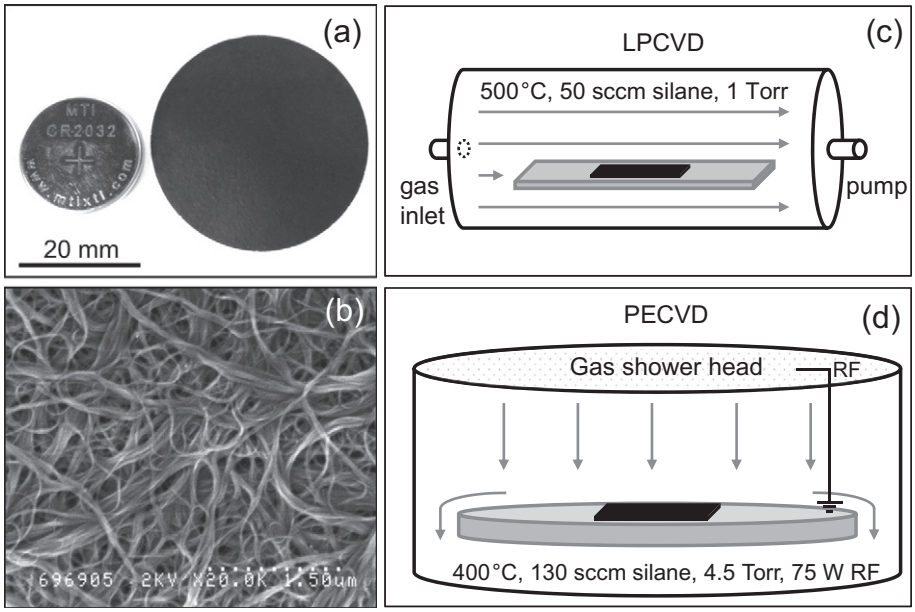

Fig. 1. (a) A freestanding SWCNT current collector is shown next to a 2032 coin cell and (b) a corresponding SEM image of the material's nanoscale morphology. Schematics of the (c) LPCVD and (d) PECVD processes are depicted (not drawn to scale). Arrows represent the direction of gas flow.

pressure was 4.5 Torr. The plasma was maintained by a 75 W RF field at 13.6 MHz. Pure silane gas flow was 130 sccm, and deposition times were between 100 and 1200 s. Samples were masked to coat only one side of the SWCNT paper. Si-SWCNT samples fabricated by PECVD are equally flexible after Si deposition, though fine cracks in the Si film can be observed. Nevertheless, the excellent electrochemical performance suggests that these cracks do not reduce the electrode performance.

2.2. Electrode characterization

Scanning electron microscope (SEM) images were collected with a Hitachi S-900 High Resolution Near Field FE-SEM, which was operated at 2 kV. Raman spectra were collected with a Jobin Yvon Horiba LabRAM HR Raman Microscope using a 633 nm HeNe source.

2.3. Electrochemical testing

Si-SWCNT anodes were tested in 2032 coin cells opposite pure lithium chips. Coin cells were assembled in an argon filled glovebox, with a Celgard 2325 separator between the electrodes. The electrolyte was 1.2 M $LiPF_6$ (Sigma Aldrich) in a 3:7 mixture of ethylene carbonate (EC) and ethyl methyl carbonate (EMC) (Novolyte Technologies, Inc.). An Arbin Instruments BT-2000 was used to galvanostatically cycle cells at 27 °C. Two conditioning cycles at an effective C-rate of C/20 were performed with a 5 mV to 3 V vs. Li/Li^+ voltage window, and subsequent cycles were at an effective C-rate of C/10 with a 5 mV to 1.5 V vs. Li/Li^+ voltage window. Full cells were also fabricated for cycle testing, where capacity matched $LiNi_{0.8}Co_{0.1}Al_{0.1}O_2$ (NCA) cathodes were paired with Si-SWCNT anodes in coin cells. The full cells received three conditioning cycles at a target C-rate of C/10, based on the target cell capacity. The full cells were then cycled at 40% depth-of-discharge (DOD) relative to the discharge energy on the third conditioning cycle; the charge rate was ∼C/2, and the discharge rate was ∼2C/3, with both steps controlled by constant power.

2.4. Postmortem analysis

Cells were prepared for postmortem analysis after cycling 1 and 7 cycles (i.e., 2 conditioning + 5 regular cycles). The 1 cycle cells were stopped after lithium extraction to 3 V vs. Li/Li^+, and the 7 cycles cells were stopped after lithium extraction to 1.5 V vs. Li/Li^+. Cells were carefully disassembled with a Hohsen Corp. Coin Cell Disassembling Tool. The cycled Si-SWCNT anodes were harvested, without rinsing, and dried in a vacuum oven at 100 °C overnight to remove residual electrolyte. SEM and Raman spectroscopy were used to characterize changes in Si surface morphology and Si crystallinity, respectively.

3. Results & discussion

3.1. SEM & Raman characterization

3.1.1. SEM

SEM images in Fig. 2 show that the morphology of Si films deposited by LPCVD (LPCVD-Si) and PECVD (PECVD-Si) are markedly different. LPCVD deposits a conformal Si layer onto the SWCNT network, whereas PECVD deposited Si forms more of a thin film coating, at similar Si loadings. This difference can be seen by comparing Fig. 2a (LPCVD) and Fig. 2d (PECVD) to an uncoated SWCNT paper (Fig. 1b). In Fig. 2a, the SWCNT bundle morphology is clearly retained at a 30% Si loading w/w, however, the PECVD sample in Fig. 2d has no visible mesopores or SWCNT bundles remaining at a Si loading of 26% w/w. At higher Si loadings, the Si-SWCNT morphology of LPCVD-Si changes as underlying SWCNT bundles are coated and mesopores are filled, but mesopores are still evident (see Fig. 2b–c). For PECVD-Si-SWCNT samples, the surface morphologies show a contiguous thin film at all Si loadings tested, three of which are shown in Fig. 2e–f, with increasing Si thickness and feature size observed with increasing deposition time. Throughout this paper, "low Si loading" will refer to samples that are 25–30% Si w/w (Fig. 2a and 2d), "medium Si loading" will refer to samples that are 50–55% Si w/w (Fig. 2c and e), and "high Si loading" will refer to samples that are 65–70% Si w/w (Fig. 2c and f).

The differences in Si film morphology are attributed to the PECVD technique depositing Si faster than the LPCVD technique, and that the deposition is more line-of-sight. These results suggest that the mesopores from the SWCNT bundles are filled rapidly during PECVD deposition, which causes a transition from a conformal type Si coating to a thin film coating. An important consequence of this difference is that more Si is able to deposit inside the SWCNT network with LPCVD deposition, because the gaseous silane precursor can continue to diffuse into the network until the mesopores have been filled with Si. Visual inspection also reveals that, despite masking, LPCVD-Si-SWCNT samples get progressively more Si coloration on the back side of the electrode with increasing deposition time. In contrast, the back side of Si-SWCNT fabricated by PECVD remains black, and no Si is detected by Raman, supporting the notion that silane is unable to diffuse through the SWCNT network after the establishment of a Si thin film.

3.1.2. Raman

Raman spectroscopy provides insight into the crystallization state of silicon [21] and Fig. 3 summarizes Raman spectra for each of the Si-SWCNT electrodes fabricated. Fig. 3a shows spectra for LPCVD-Si at low (i.e., 30% Si w/w, 15 min deposition), medium (i.e., 55% Si w/w, 25 min deposition), and high (i.e., 65% Si w/w, 40 min deposition) Si loadings. In each case, SWCNT and Si features are clearly present, and it can be observed that the intensity of the SWCNT features is inversely proportional to the Si loading. SWCNT radial breathing modes (RBMs) are visible below 300 cm^{-1}, and well-defined G-band (∼1580 cm^{-1}) and G′-band (∼2600 cm^{-1}) features are also observed. The broad Si feature that is present for each Si loading is highlighted in Fig. 3b, with a peak around 470 cm^{-1}, which is characteristic of amorphous Si (a-Si) [21]. Highly crystalline Si (c-Si) would have a narrow peak at 521 cm^{-1}. This is consistent with the literature, since LPCVD deposition is expected to produce amorphous silicon under the deposition conditions used [22].

Fig. 3c has representative Raman spectra of Si-SWCNT electrodes prepared by PECVD deposition at low (i.e., 26% Si w/w, 200 s deposition), medium (i.e., 55% Si w/w, 840 s deposition), and high (i.e., 68% Si w/w, 1200 s deposition) Si loadings. At the low Si loading, SWCNT Raman features are weak, somewhat comparable to the high Si loading LPCVD sample. At medium and high PECVD-Si loadings, SWCNT features have disappeared, which is due to the fact that the Si film that forms during PECVD deposition is too thick for SWCNT excitation. Unlike the LPCVD material, the PECVD material shows a mixture of amorphous and semi-crystalline Si across the sample, as highlighted by representative spectra in Fig. 3d. Raman spectra were taken from several spots on each sample, and it was observed that the likelihood of finding c-Si increases with Si loading.

3.2. Electrochemical characterization

3.2.1. First and second cycle voltage profiles

Si-SWCNT electrodes were tested vs. lithium to assess their lithium ion storage capacity. Voltage profiles from the first and

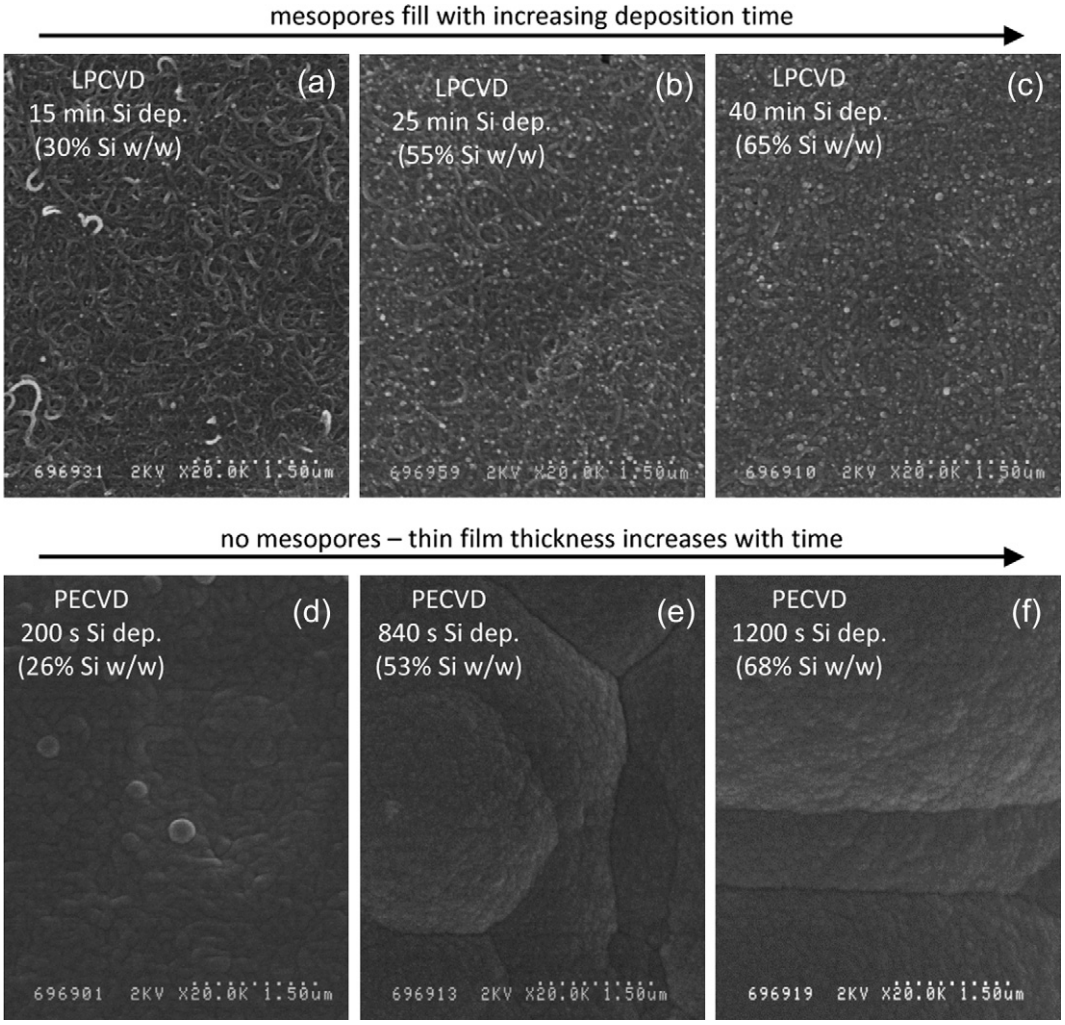

Fig. 2. (a–c) SEM images from LPCVD deposition of Si. The SWCNT bundle mesopores are progressively filled with Si at higher Si loadings. (d–f) SEM images of Si-SWCNT samples from PECVD deposition of Si. A textured thin film morphology is observed over the range of Si loadings.

second cycles of representative cells are shown in Fig. 4. The first two cycles are conditioning cycles at an effective C/20 rate, and the voltage window is 5 mV to 3 V vs. Li/Li^+. There is an increase in lithium extraction capacity and coulombic efficiency as the Si loading increases from ~25–30% Si w/w (Fig. 4a/b), to ~55% Si w/w (Fig. 4c/d), and to ~65–70% Si w/w (Fig. 4e/f). For LPCVD-Si-SWCNT electrodes, extraction capacities range between 964 mAh g^{-1} and 1673 mAh g^{-1}. At the same Si weight loadings, PECVD-Si-SWCNT demonstrates 30–50% higher extraction capacities ranging between 1284 mAh g^{-1} and 2490 mAh g^{-1} (note that these gravimetric capacities are for the full electrode mass, comprising Si and SWCNT current collector).

Solid electrolyte interphase (SEI) formation on the SWCNT current collector is observed as a plateau at 0.8–0.9 V during the first cycle insertion (Fig. 4). The amount of lithium that goes into SEI formation is irreversible capacity [2]. The SEI loss for CVD Si-SWCNT anodes is observed to decrease as the Si loading increases, as evident across the top and bottom row of Fig. 4. There appear to be subtle differences in the insertion/extraction profiles of LPCVD and PECVD deposited Si, but Si forms amorphous Li–Si phases at room temperature [3,23], so these cannot be attributed to changes in Li–Si crystal phase. First cycle coulombic efficiency is 39% for LPCVD and 46% for PECVD fabricated Si-SWCNT electrodes at 25–30% Si w/w (Fig. 4a/b). At Si loadings of ~55% w/w, the coulombic efficiency improves to 73% for LPCVD-Si-SWCNT and 69% for PECVD-Si-SWCNT electrodes (Fig. 4c/d). At 65–70% Si w/w, the coulombic efficiencies show a slight improvement to 76% for LPCVD and 75% for PECVD (Fig. 4e/f). As the Si loading increases, a reduction in accessible surface area of the SWCNT network would be consistent with SEM images, thus decreasing the excessive SEI formation from the pristine SWCNT.

In the second cycle, the SEI plateau near 0.8 V disappears from the voltage profile, significantly improving the second cycle coulombic efficiencies (Fig. 4, red insertion curve). The coulombic efficiency at 25–30% Si w/w dramatically increases to 82% for LPCVD-Si-SWCNT and 87% for PECVD-Si-SWCNT in the second cycle. The LPCVD-Si-SWCNT electrodes at 55% and 65% Si w/w improved to near 100% and 98% coulombic efficiency, respectively, on the second cycle. The PECVD-Si-SWCNT electrodes at 53% and 68% Si w/w improved to 87% and 95% coulombic efficiency, respectively. Therefore, after the initial conditioning cycles, the coulombic efficiency for both LPCVD- and PECVD-Si-SWCNT anodes is greatly improved.

3.2.2. *Coulombic efficiencies as a function of Si deposited*

Fig. 5 shows a plot of first cycle coulombic efficiencies as a function of the areal density of Si deposited for both LPCVD and PECVD techniques. Also provided is a data point for purified SWCNT

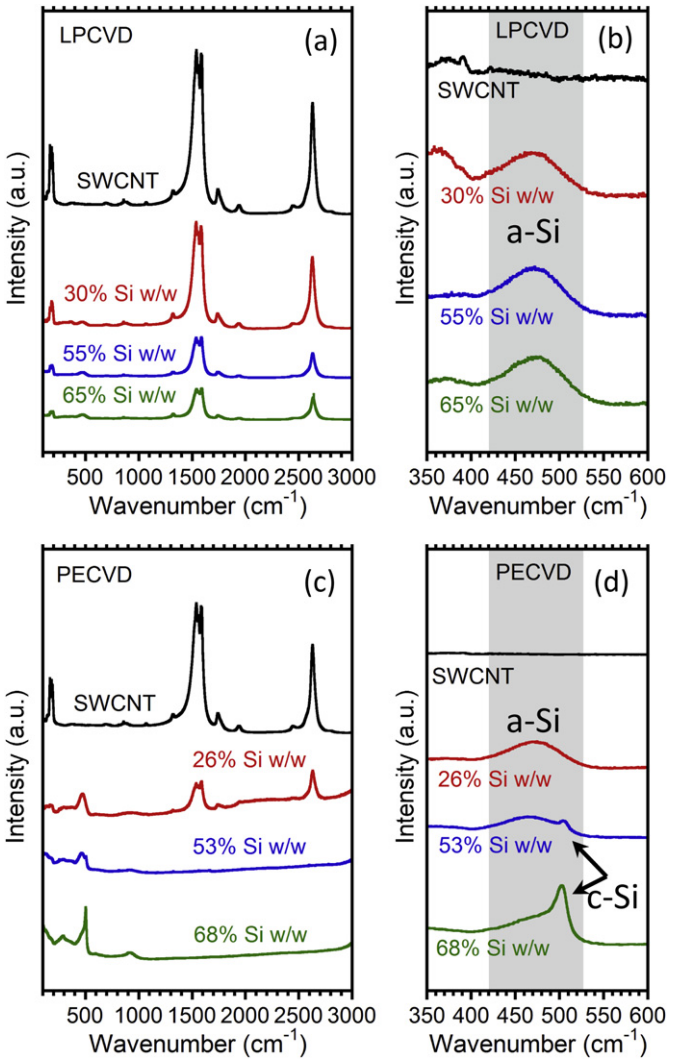

Fig. 3. (a) Raman spectra for LPCVD deposited Si-SWCNT show attenuation of the characteristic SWCNT signal and emergence of the Si signal. (b) The Si region (350–600 cm^{-1}) shows that the Si is amorphous (broad peak at ~470 cm^{-1}), with no indication of crystalline Si domains (at 520 cm^{-1}). (c) Raman spectra for PECVD deposited Si-SWCNT show a suppressed SWCNT signal at lower exposures, due to the thin film Si morphology. (d) The PECVD material, however, shows evidence of both amorphous and crystalline domains, with more crystallinity observed at higher Si loadings.

paper without Si, which typically has poor coulombic efficiencies around 20% [5,24]. Deposition of silicon to create Si-SWCNT electrodes can dramatically improve the first cycle coulombic efficiency to >75–80%. Most of the improvement occurs below 1 mg cm^{-2} Si (i.e., ~50% Si), with only minor improvement at higher Si loadings. This trend is indicated by the dashed line in Fig. 5. SEI formation is a function of electrode surface area, which is reduced by the filling of mesopores during silicon deposition. Improvements in coulombic efficiency saturate above 1 mg cm^{-2} Si, when a large fraction of the mesopores have been filled and further Si deposition leads to increased Si coating thickness. The data in Fig. 5 indicates that both CVD methods result in similar coulombic efficiencies, despite the difference in Si film morphology (i.e., conformal coating vs. thin film).

3.2.3. Si-only extraction capacities

Fig. 6a provides a summary of electrode extraction capacity data from the 3rd cycle, after 2 conditioning cycles, for electrodes fabricated with Si loadings ranging from 0.3 to 2.2 mg cm^2. The voltage range for the Si-SWCNT electrodes is 5 mV to 1.5 V vs. Li/Li^+ and the rate is an effective C/10 rate. The results show that the total electrode capacity of PECVD-Si-SWCNT anodes is consistently higher than LPCVD-Si-SWCNT electrodes. The greater variance in extraction capacities, determined from testing multiple samples, at higher Si loadings for LPCVD-Si-SWCNT electrodes is attributed to Si deposition on the back side of the electrodes (Fig. 6a). Raman spectroscopy was used to confirm that no measurable Si deposition occurred on the back side of PECVD-Si-SWCNT electrodes. The difference in performance becomes even more apparent when the 3rd cycle (after 2 conditioning cycles) extraction capacity for only Si is plotted against the amount of Si deposited (Fig. 6b). The Si-only extraction capacities are calculated using the following equation:

$$C_{Si} = \frac{C_{TOT} - (C_{SWCNT})(w_{SWCNT})}{w_{Si}}$$

where C_{Si} is the Si-only capacity, C_{TOT} is the total electrode capacity, w_{SWCNT} is the weight fraction that is SWCNT, w_{Si} is the weight fraction that is Si, and C_{SWCNT} is the extraction capacity of the SWCNT paper. C_{SWCNT} depends on the electrolyte, and was experimentally determined to be 130 mAh g^{-1} in 1.2 M $LiPF_6$, 3:7 EC:EMC electrolyte for pure SWCNT electrodes with a 1.5 V vs. Li/Li^+ cutoff. It is apparent from Fig. 6a and b that the PECVD-Si-SWCNT electrodes have higher electrode capacities and Si active material capacities.

Across the full range of Si loadings tested, LPCVD-Si-SWCNT has Si-only specific capacities of 1500–2000 mAh g^{-1}, though there is more experimental variability at higher Si loadings. Above ~0.7 mg cm^{-2} Si, PECVD-Si-SWCNT has Si-only specific capacities of 2700–3000 mAh g^{-1}, which is 50% better than what is observed for the LPCVD-Si-SWCNT. Below ~0.7 mg cm^{-2} Si, the Si-only specific capacity for PECVD-Si-SWCNT increases almost linearly. In fact, at Si loadings below 0.5 mg cm^{-2}, the Si-only specific capacity of PECVD-Si-SWCNT is roughly double that of LPCVD-Si-SWCNT Fully lithiated Li–Si alloys of $Li_{15}Si_4$ (3580 mAh g^{-1}) and $Li_{22}Si_5$ (4200 mAh g^{-1}) are theoretically predicted [25], which suggests that there is some mixture of these two alloy states for the samples that have extraction capacities above 3600 mAh g^{-1}, such as the PECVD-Si-SWCNT electrodes with <0.4 mg cm^{-2} Si.

The best performing Si-SWCNT sample had a Si-only specific capacity of 3780 mAh g^{-1} at a 26% Si loading, which is higher than values found in the literature for related Si-CNT systems. Recently published results [11–15,26,27] all have Si-only extraction capacities below 3500 mAh g^{-1}, with the single exception being the work by Chou et al. [28]. In that study, a specific capacity of 3700 mAh g^{-1} was demonstrated at a 2.2% Si loading, but the performance dropped significantly at a higher Si loading of 11% [28]. Most of the reported results have Si-only extraction capacities in the range 1500–3000 mAh g^{-1}, which is consistent with the present results for LPCVD-Si-SWCNT and higher weight loadings of PECVD-Si-SWCNT. The only two reports that indicated Si-only extraction capacities over 3000 mAh g^{-1} at Si loadings >2% [12,27] did not utilize the free-standing electrode approach, and have metal current collectors, which lessens the impact on energy density in a full battery. In fact, 2.2 mg cm^{-2} Si on 20 μm thick copper foil (16.4 mg cm^{-2}), with a Si extraction capacity of 3000 mAh g^{-1}, would have a total electrode extraction capacity of approximately 350 mAh g^{-1}. This is nearly an order of magnitude lower than the 2000 mAh g^{-1} achieved with a free-standing PECVD-Si-SWCNT anode (i.e., no copper current collector). The free-standing PECVD-Si-SWCNT anodes presented here have demonstrated exceptional electrochemical performance compared to LPCVD-Si-SWCNT anodes, Si-Copper anodes, and state-of-the-art graphitic anodes.

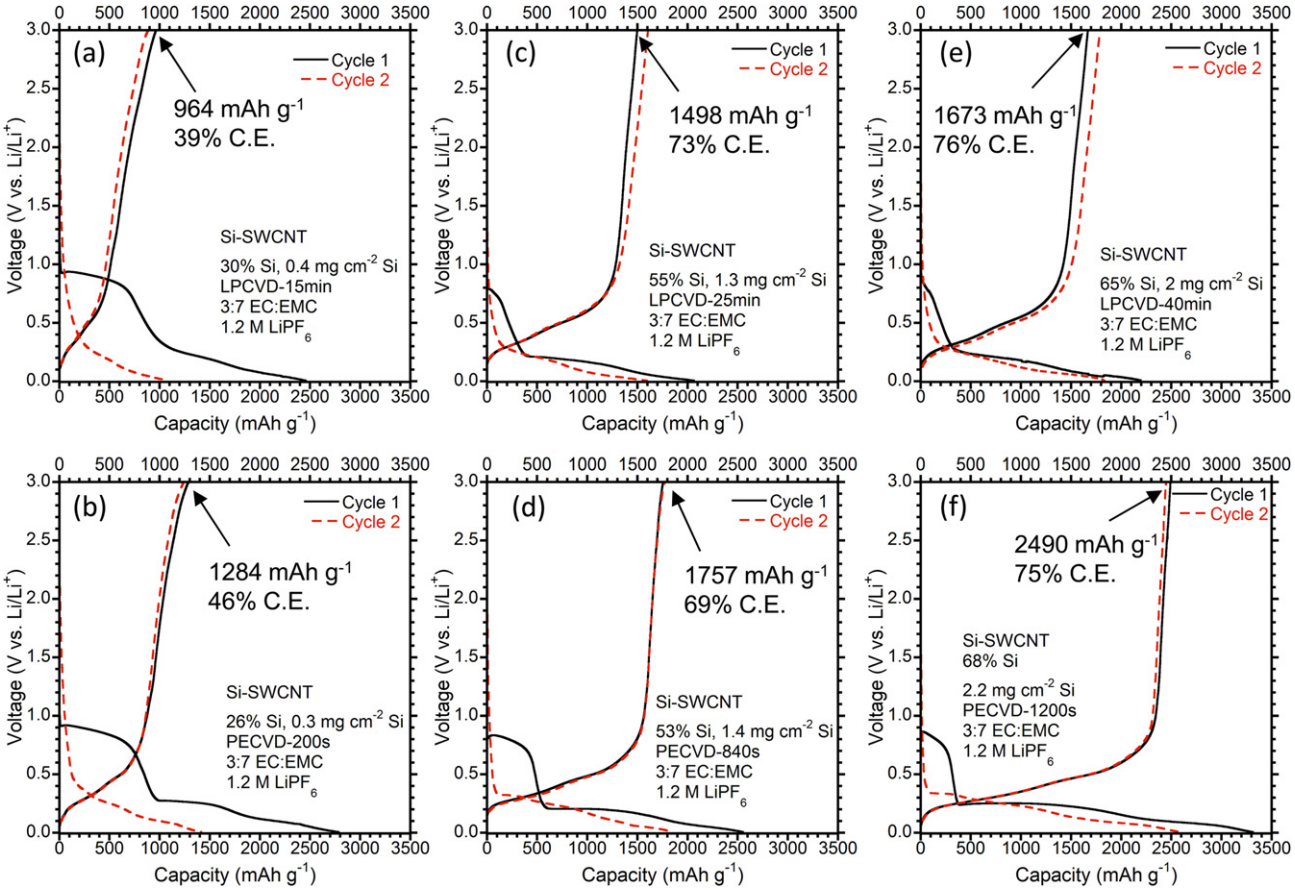

Fig. 4. Insertion/extraction profiles from the first two cycles of both LPCVD (top) and PECVD (bottom) deposited Si-SWCNT anodes. (a–b) Si loadings of 25–30%, (c–d) Si loadings of ~55%, and (e–f) Si loadings of 65–70%. SEI formation on the SWCNT surface manifests as a voltage plateau at 0.8–0.9 V vs. Li/Li^+ on the first cycle.

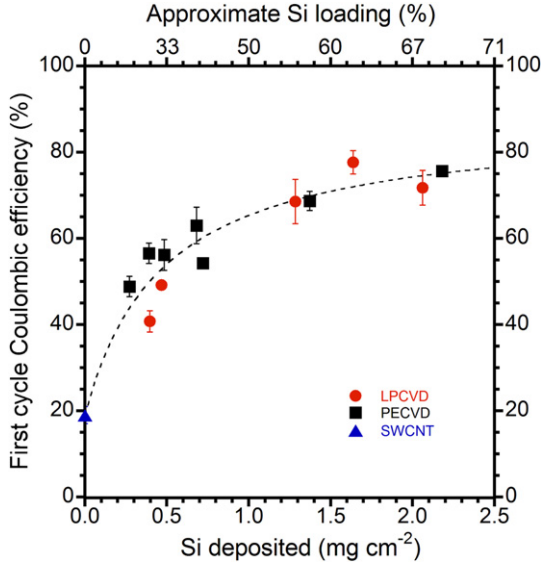

Fig. 5. Coulombic efficiencies for LPCVD (red circles) and PECVD (black squares) Si-SWCNT electrodes as a function of Si deposited. Error bars represent the standard deviation in measured coulombic efficiency values, based on 2–4 samples at each Si loading. Pure SWCNT (blue triangle) is shown for a 0% Si loading. (For interpretation of the references to color in this figure legend, the reader is referred to the web version of this article.)

These results underscore the importance of carefully choosing a CVD method when engineering nano-structured electrodes for batteries. Moreover, the Si-only extraction capacity has been show to vary significantly with the Si loading, which has not been systematically studied previously.

3.2.4. *Cycling of PECVD-Si-SWCNT anodes vs. lithium*

Since the PECVD-Si-SWCNT anodes are superior to the LPCVD-Si-SWCNT anodes in total electrode extraction capacity, Si-only extraction capacity, and cycling stability, only results from cycling PECVD-Si-SWCNT anodes vs. lithium at the low Si (26%), medium Si (53%), and high Si (68%) loadings are presented. Fig. 7a shows the cycling performance of these anodes vs. lithium at an approximate C/10 rate and 100% depth-of-discharge (DOD). The low Si loading cell displays no cycle fade over 20 cycles, with a total electrode extraction capacity of ~1000 mAh g^{-1}. The medium Si loading cell also cycles well, with a starting total electrode extraction capacity of ~1500 mAh g^{-1}, and a 10% capacity fade over 20 cycles. In contrast, the high Si loading sample does not cycle as well, and has significant variations in extraction capacity from cycle to cycle. The starting total electrode capacity is ~1850 mAh g^{-1}, and there is a 16% capacity fade over 20 cycles. There has been no attempt to optimize the supporting SWCNT current collector, but a thicker SWCNT substrate would likely be able to accommodate higher Si loadings (>2 mg cm^{-2}) during the large volumetric changes of the Si film during lithiation/delithiation. Overall, these results show promising cycling vs. lithium at *electrode* capacities of 1000–1500 mAh g^{-1} without any electrode optimization.

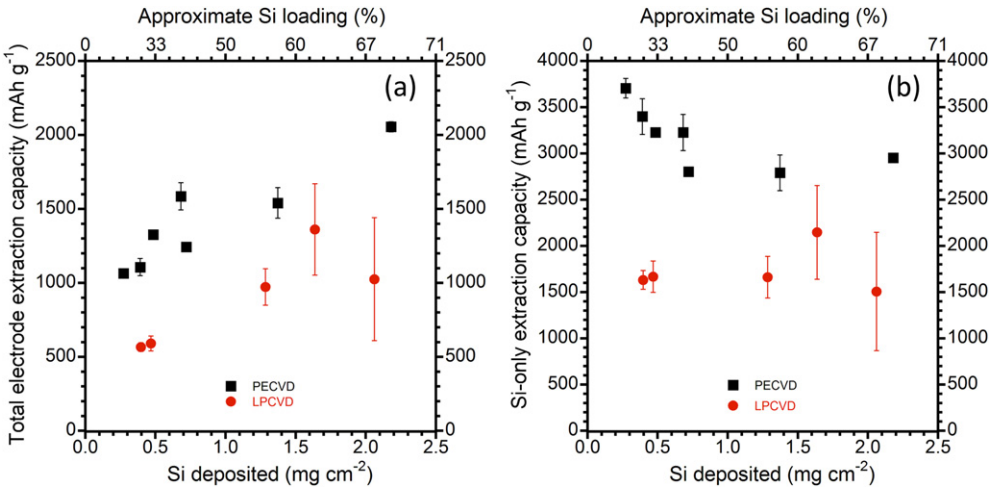

Fig. 6. (a) Total electrode extraction capacity plotted against the amount of Si deposited for both LPCVD (red circles) and PECVD (black squares), and (b) the Si-only extraction capacity plotted against the amount of Si deposited. Error bars represent the standard deviation in extraction capacities, based on 2–4 samples at each Si loading. (For interpretation of the references to color in this figure legend, the reader is referred to the web version of this article.)

3.2.5. Cycling of PECVD-Si-SWCNT anodes in full cells

Full cells were fabricated to determine how well Si-SWCNT anodes cycle when paired with a $LiNi_{0.8}Co_{0.1}Al_{0.1}O_2$ (NCA) cathode. Similar to anode testing vs. lithium, only PECVD-Si-SWCNT anodes at the low Si (26%), medium Si (53%), and high Si (68%) loadings were fabricated into full cells. The target areal capacities for these cells were ~2 mAh cm^{-2}, ~4 mAh cm^{-2}, and ~8 mAh cm^{-2} for the low Si loading, medium Si loading, and high Si loading, respectively. After three conditioning cycles, the cells were cycled at a target 40% DOD, with relatively strenuous charge and discharge rates of ~C/2 and ~2C/3, respectively. It should be noted that the real capacities were lower than the design capacities due to the large irreversible first cycle loss for Si-SWCNT anodes, which could be mitigated using pre-lithiation strategies in commercial production.

Fig. 7b shows that cycling stability under these conditions is excellent for low and medium Si loadings. In this plot, the stability of the anodes is monitored by the end-of-discharge voltage at 40% DOD, which will decrease as the cell performance degrades. After the three conditioning cycles, 40% DOD corresponds to an end-of-discharge voltage of approximately 3.5–3.6 V for these cells. After 100 cycles, the low and medium Si loading cells' end-of-discharge voltage is within 0.05 V of the initial value, demonstrating stable cycling under these conditions. In contrast, the high Si loading cell did not perform as well, and the cell was stopped after 55 cycles, when the end-of-discharge voltage reached 2.5 V. This demonstrates that PECVD-Si-SWCNT free-standing anodes perform well at commercially viable areal capacities (i.e. 2-4 mA h cm^{-2}), and for applications where reduced DOD cycling is used to extend cell/battery cycle life.

3.3. Postmortem analysis

3.3.1. SEM

In order to gain further insight into the morphological changes that happen to the Si-SWCNT electrodes during early cycling, several coin cells were disassembled for postmortem analysis after 1 and 7 cycles (i.e. 2 conditioning + 5 regular, to a lithium extraction of 3 V vs. Li/Li^+). SEM images of postmortem samples are shown for both CVD techniques in Fig. 8 (low Si loading), Fig. 9 (medium Si loading), and Fig. 10 (high Si loading). For low Si loadings (Fig. 8), there appears to be minimal, but evident change in

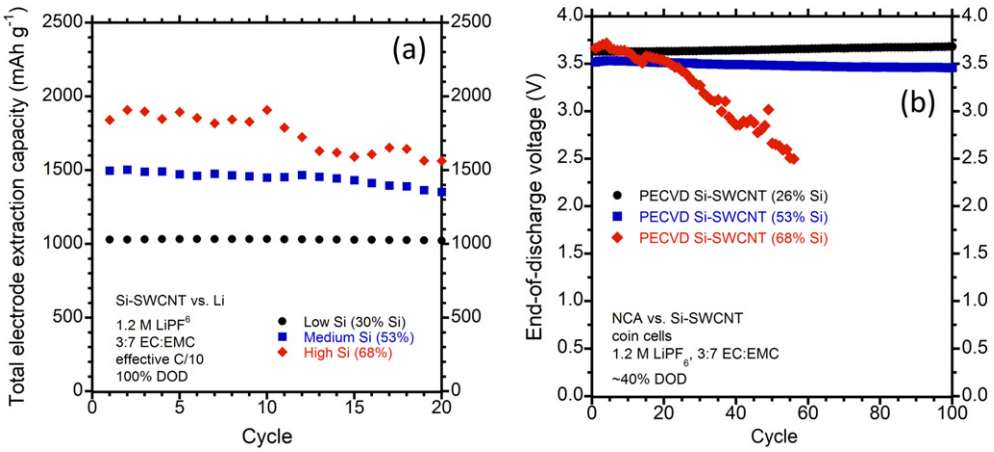

Fig. 7. (a) Cycling data for PECVD-Si-SWCNT anodes vs. lithium at 100% DOD, with low Si (black circles), medium Si (blue squares), and high Si (red diamonds) loadings, and (b) cycling data from full cells (NCA vs. PECVD-Si-SWCNT). Full cells were cycled at 40% DOD, with charge and discharge rates of ~C/2 and ~2C/3, respectively, and the end-of-discharge voltage is plotted vs. cycle number. (For interpretation of the references to color in this figure legend, the reader is referred to the web version of this article.)

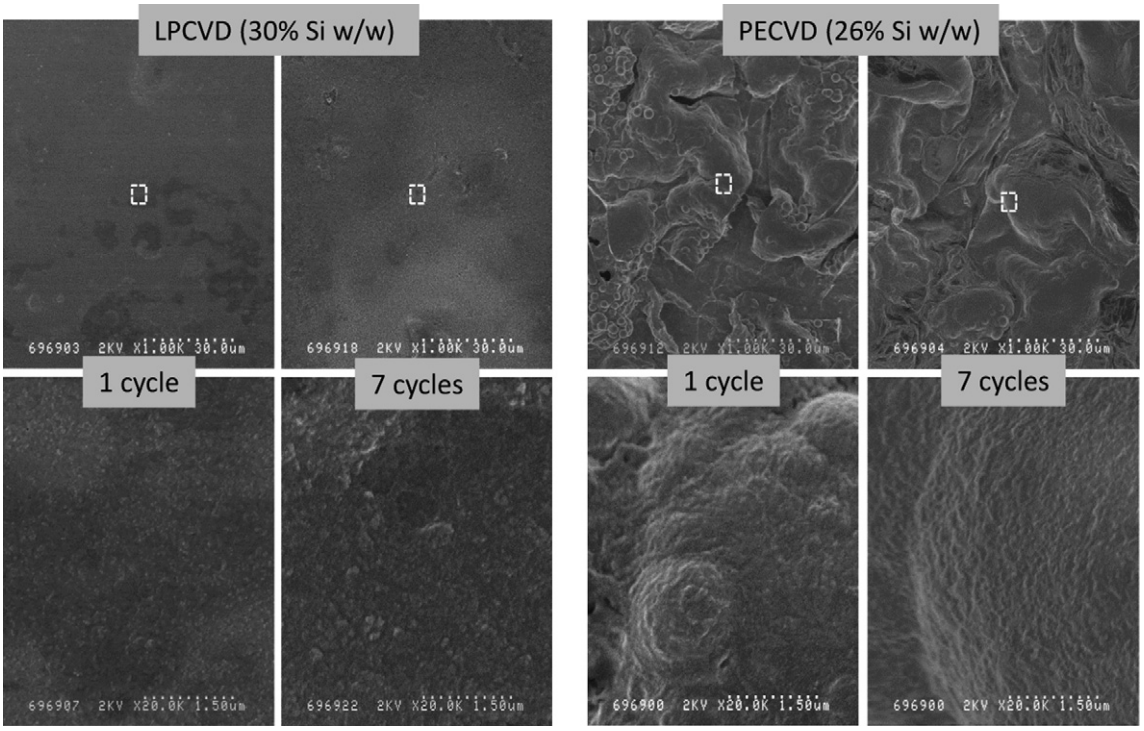

Fig. 8. Postmortem SEM images of Si-SWCNT anode surfaces at 1,000× magnification (top row) and 20,000× magnification (bottom row), where the Si loading is 30% Si w/w for LPCVD and 26% Si w/w for PECVD. Coin cells were tested for 1 cycle and 7 cycles (2 conditioning + 5 regular) before disassembly. White dashed boxes on 1,000× magnification images (top row) indicate the location of the 20,000× magnification images (bottom row).

the LPCVD-Si film after 1 and 7 cycles at 1,000× magnification. At 20,000× magnification, the change in surface texture of the cycled LPCVD-Si-SWCNT is observed more clearly. The SWCNT bundle morphology that was easily visible before cycling (Fig. 2a) is obscured by a uniformly nano-textured surface. Reorganization of Si and/or SEI formation may be the source of this change in surface morphology for LPCVD-Si-SWCNT electrodes. The PECVD-Si films at low Si loadings are structurally quite different from LPCVD-Si films

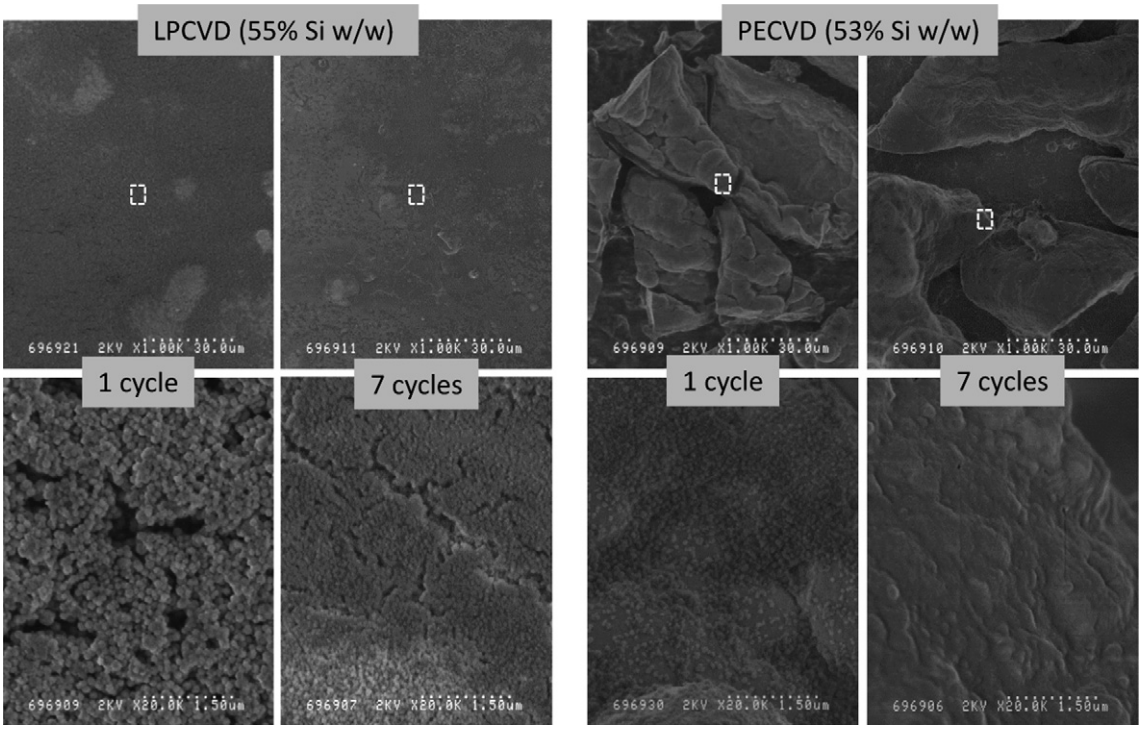

Fig. 9. Postmortem SEM micrographs of Si-SWCNT anode surfaces at 1,000× magnification (top row) and 20,000× magnification (bottom row), where the Si loading is 55% Si w/w for LPCVD and 53% Si w/w for PECVD. Coin cells were tested for 1 cycle and 7 cycles (2 conditioning + 5 regular) before disassembly. White dashed boxes on 1,000× magnification images (top row) indicate the location of the 20,000× magnification images (bottom row).

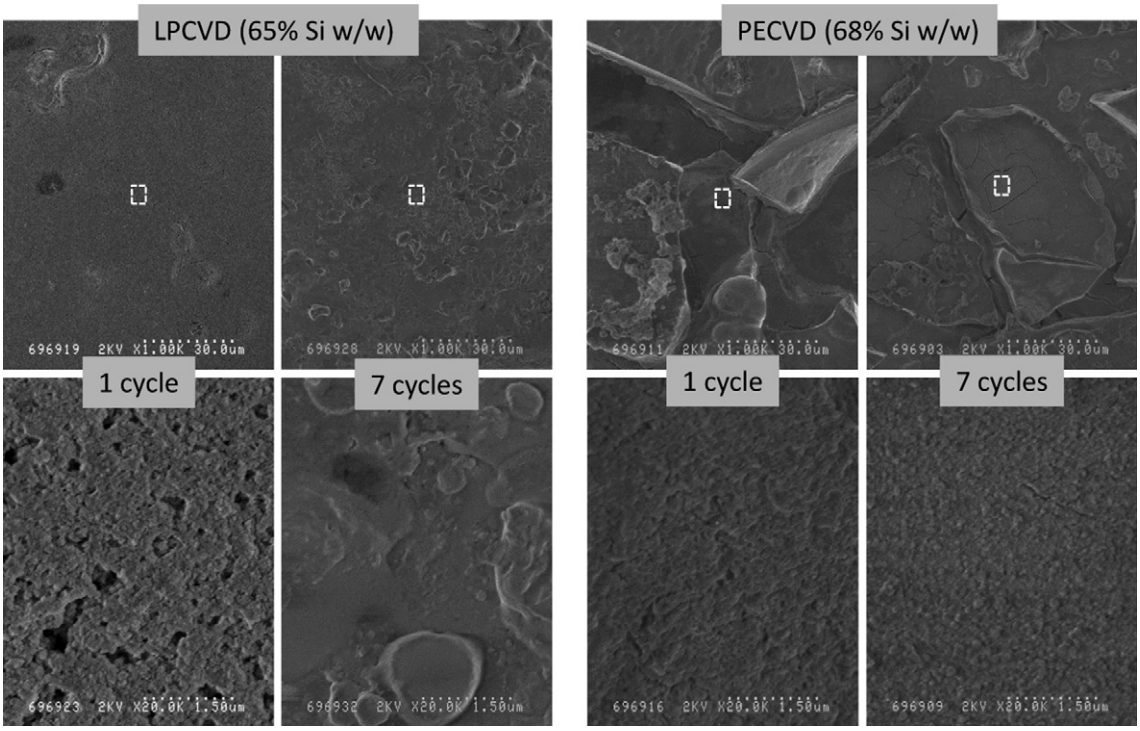

Fig. 10. Postmortem SEM micrographs of Si-SWCNT anode surfaces at 1,000× magnification (top row) and 20,000× magnification (bottom row), where the Si loading is 65% Si w/w for LPCVD and 68% Si w/w for PECVD. Coin cells were tested for 1 cycle and 7 cycles (2 conditioning + 5 regular) before disassembly. White dashed boxes on 1,000× magnification images (top row) indicate the location of the 20,000× magnification images (bottom row).

after cycling, when imaged at 1,000× magnification (Fig. 8). After just 1 cycle, the Si thin film has fractured into agglomerated sections, on the order of 10–50 μm, that cover the entire electrode. The surface structure looks quite similar after 7 cycles at 1,000× magnification. At 20,000× magnification, it was observed that, after 1 cycle, the surface has nano-texturing on the order of 100–200 nm, similar to the LPCVD-Si.

For medium Si loadings (Fig. 9), LPCVD-Si-SWCNT electrodes look the same as the low Si loading samples at 1,000× magnification after 1 and 7 cycles. At 20,000× magnification, it appears that roughly spherical structures have formed on the electrode surface after 1 cycle, with diameters on the order of 100–200 nm. Based on recent theoretical work [29], Si nanoparticles that are <150 nm in diameter should not be pulverized on lithium insertion/extraction. Given that result, it is possible that a Si film would self-optimize to have nano-spheres of this size during cycling. However, similar structures have also been observed in postmortem studies of SWCNT electrodes without Si, so it may be a combination of SEI formation and Si structural optimization. After 7 cycles, that nano-structure is still visible, but the spherical particles have coalesced. Additionally, when compared to the as-deposited electrode (Fig. 2b), it can be seen that Si has reorganized on the surface during lithium extraction and the SWCNT bundle morphology is no longer visible. PECVD-Si-SWCNT electrodes with medium Si loadings closely resemble the low Si loading samples after 1 and 7 cycles, with some variation in the surface texture at high magnification. At low magnification, it is observed that the large agglomerated Si structures have better definition than at the low Si loading.

Lastly, samples with high Si loadings are shown in Fig. 10. After 1 cycle, the LPCVD sample shows a surface texture that resembles the medium Si loading sample, with similar porosity but less spherical definition. After 7 cycles, the surface roughness on the micron scale (1,000× magnification) has increased, which was previously only observed for PECVD samples. Conversely, there is less nano-texturing observed at 20,000× magnification for the LPCVD sample. The PECVD-Si-SWCNT samples at high Si loading are consistent with samples at lower Si loadings, both in nano-texturing and the 10–50 μm agglomerate structures.

Clearly there are major differences in the evolution of the LPCVD-Si and PECVD-Si films during cycling. LPCVD-Si undergoes surface reorganization and can form a nano-sphere morphology/texture. PECVD-Si films deposit with a more crystalline structure and fracture into agglomerates that are still able to efficiently insert/extract lithium, while also gaining some surface texturing. It is suggested that the mechanical compliance of the SWCNT free-standing current collector is able to accommodate the expansion/contraction of the Si while maintaining acceptable electrical contact, which prevents performance degradation of the PECVD-Si-SWCNT due to the large agglomerate structures.

3.3.2. Raman

Postmortem samples with low, medium, and high Si loadings were also characterized by Raman spectroscopy (Fig. 11). LPCVD-Si-SWCNT spectra have consistent features prior to cycling and after 1 and 7 cycles (see Fig. 10a, c, and e). The broad peak at ~470 cm^{-1} is characteristic of amorphous Si, without any indications of crystalline domains in the Si film. After cycling, the intensity of the SWCNT G-band, G′-band, and RBMs are observed to decrease in intensity, relative to the a-Si peak, while there is an increase in the D-band intensity. These changes are likely due to SEI formation affecting the vibrational modes of the SWCNTs and possibly chemical bonding at the SEI-SWCNT interface [8]. The similarities between postmortem Raman spectra at varying Si loadings are consistent with the small changes in surface morphology that were observed in postmortem SEM images for LPCVD-Si-SWCNT.

In contrast, the PECVD-Si-SWCNT spectra change more significantly over 7 cycles, as shown in Fig. 10b, d, and f. As-deposited, the SWCNT features are minimally present at a low Si loading (Fig. 11b), and not present at medium and high Si loadings (Fig. 10d and f, respectively) because of the Si thin film that forms during

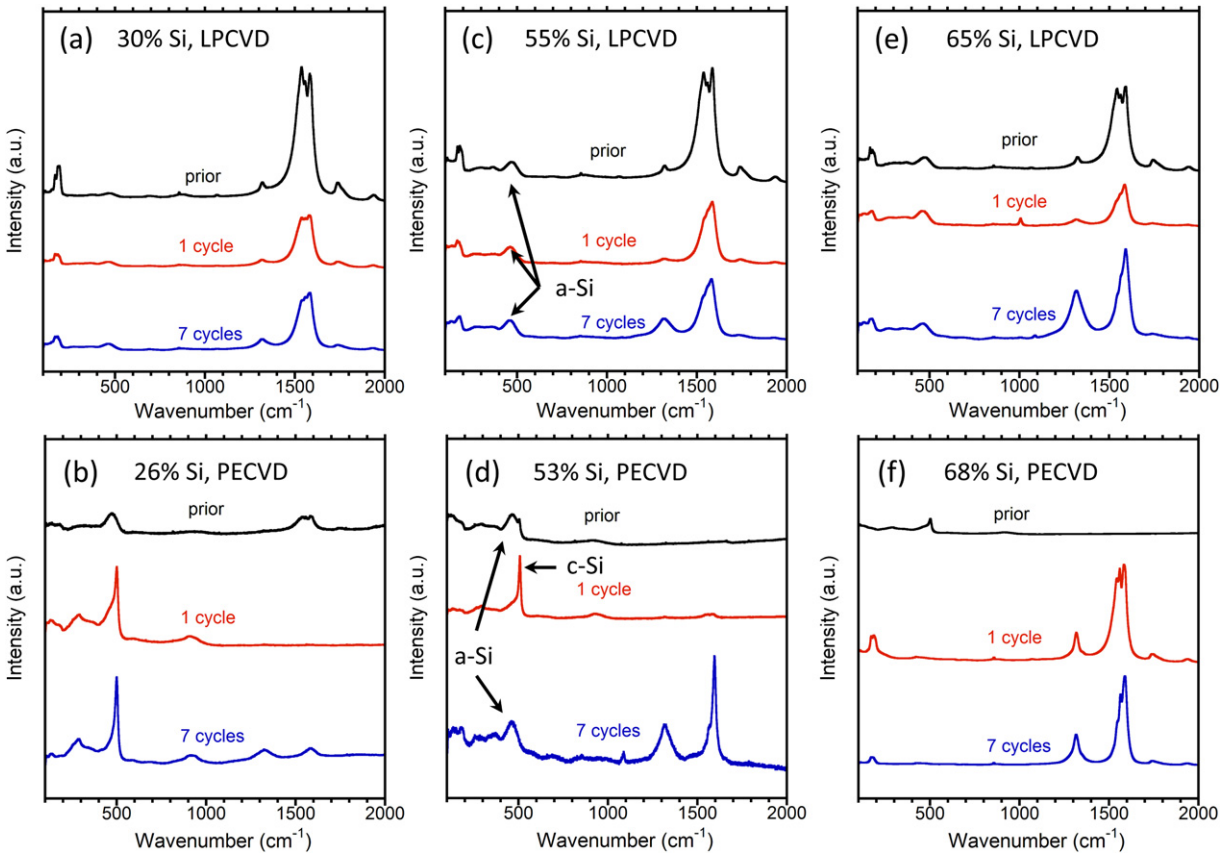

Fig. 11. Postmortem Raman spectra for both LPCVD (top) and PECVD (bottom) deposited Si-SWCNT anodes. (a–b) Si loadings of 26–30%, (c–d) Si loadings of 53–55%, and (e–f) Si loadings of 65–68%. For each LPCVD-Si and PECVD-Si loading, spectra are shown prior to cycling, after 1 cycle, and after 7 cycles.

deposition. In the low Si loading samples, the SWCNT spectrum is weak, but present, prior to cycling and after 7 cycles (Fig. 11b). After 1 and 7 cycles, there is a strong peak at ~500 cm^{-1} resulting from a mixture of a-Si and c-Si after lithium extraction due to recrystallization of the Si, which has been reported previously [30]. For the medium Si loading samples (Fig. 11d), the c-Si peak is observed after 1 cycle, but not after 7 cycles. Also, the SWCNT features are significantly more pronounced after 7 cycles, which is likely due to increased spacing between Si agglomerates, which allows the excitation laser to probe the underlying SWCNTs. In the high Si loading samples (Fig. 11f), more pronounced c-Si is observed after deposition (prior to cycling), but only a weak Si signal could be detected after cycling, relative to the SWCNT signal. As with the LPCVD-Si-SWCNT electrodes, there is an increase in the intensity of the D-band after cycling. These postmortem Raman results, along with the postmortem SEM images, indicate that the reorganization of Si on the LPCVD-Si-CNT and PECVD-Si-CNT anodes leads to dramatically different electrode morphology and Si crystallinity during the first few cycles. Despite the larger morphological changes and varying degree of Si crystallinity, PECVD-Si-SWCNT anodes consistently demonstrate higher lithium extraction capacities while maintaining similar coulombic efficiencies to LPCVD-Si-SWCNT anodes.

4. Conclusion

The results presented herein show that the choice of CVD deposition method can have a significant impact on Si-SWCNT electrode morphology and performance. PECVD-Si-SWCNT electrodes demonstrated higher extraction capacities (total electrode and Si-only) at comparable Si weight loadings. PECVD deposited Si-SWCNT electrodes have demonstrated the best Si-only extraction capacity reported to date (3780 mAh g^{-1}). At low Si loadings (i.e., <0.4 mg cm^{-2} Si), the Si-only extraction capacities exceed 3580 mAh g^{-1} ($Li_{15}Si_4$ phase), which strongly suggests that a mixture of the $Li_{15}Si_4$ and $Li_{22}Si_5$ phases are formed during lithiation of PECVD-Si-SWCNT electrodes. Full cell cycling of PECVD-Si-SWCNT anodes vs. NCA cathodes demonstrated stable cycling at 40% DOD for 100 cycles with minimal performance degradation, when the anode areal capacity was 2–4 mAh cm^{-2}. Postmortem analysis reveals that LPCVD-Si maintains a consistent microscale surface roughness during cycling, whereas PECVD-Si films fracture into agglomerate structures. With metal current collectors, such agglomerate structures would likely be pulverized, but the mechanically compliant SWCNT current collector is able to accommodate the large volume changes during lithium insertion/extraction. Both types of Si also exhibit nano-structuring/texturing that evolves during cycling, but is relatively stable after the first cycle.

The efficient use of Si at lower Si loadings is beneficial for reducing the amount of Si needed, while retaining total electrode extraction capacities ≥1000 mAh g^{-1}. Large scale manufacturing of CNT materials at competitive cost is now becoming a commercial reality (e.g. Nanocomp Technologies), which will help transition CNT current collectors to an application scale, and the PECVD deposition method is already used for roll-to-roll applications. The high performance of PECVD-Si-SWCNT electrodes, and potential for scalability, are promising for the development of commercially viable free-standing anodes that incorporate high capacity Si active materials.

Acknowledgments

The authors gratefully acknowledge financial support from the Department of Energy (DE-FG36-08 GO88110) and the US Government, including a grant from the Intelligence Community Postdoctoral Research Fellowship Program through funding from the Office of the Director of National Intelligence. This material is based upon work funded in whole or in part by the U.S. Government and any opinions, findings, conclusions, or recommendations expressed in this material are those of the authors and do not necessarily reflect the views of the U.S. Government. R.A.D. acknowledges graduate student funding from a GAANN fellowship through the RIT Microsystems Engineering Ph.D. program. The authors also wish to acknowledge Bruce Tolleson from the Semiconductor & Microsystems Fabrication Laboratory at RIT for his assistance with the LPCVD system.

Glossary

CNT	carbon nanotubes
CVD	chemical vapor deposition
EC	ethylene carbonate
EMC	ethyl methyl carbonate
LPCVD	low-pressure chemical vapor deposition
MWCNT	multi-walled carbon nanotube
PECVD	plasma-enhanced chemical vapor deposition
RBM	radial breathing mode
SEI	solid electrolyte interphase
SEM	scanning electron microscopy
SWCNT	single-walled carbon nanotube

References

[1] J.B. Goodenough, Y. Kim, Chem. Mater. 22 (2010) 587–603.
[2] B.J. Landi, M.J. Ganter, C.D. Cress, R.A. DiLeo, R.P. Raffaelle, Energy Environ. Sci. 2 (2009) 638–654.
[3] J. Graetz, C.C. Ahn, R. Yazami, B. Fultz, J. Electrochem. Soc. 151 (2004) A698–A702.
[4] U. Kasavajjula, C.S. Wang, A.J. Appleby, J. Power Sources 163 (2007) 1003–1039.
[5] R.A. DiLeo, M.J. Ganter, R.P. Raffaelle, B.J. Landi, J. Mater. Res. 25 (2010) 1441–1446.
[6] B.J. Landi, C.D. Cress, R.P. Raffaelle, J. Mater. Res. 25 (2010) 1636–1644.
[7] L.B. Hu, J.W. Choi, Y. Yang, S. Jeong, F. La Mantia, L.F. Cui, Y. Cui, Proc. Natl. Acad. Sci. U. S. A. 106 (2009) 21490–21494.
[8] B.J. Landi, M.J. Ganter, C.M. Schauerman, C.D. Cress, R.P. Raffaelle, J. Phys. Chem. C 112 (2008) 7509–7515.
[9] J.Y. Eom, H.S. Kwon, ACS Appl. Mater. Interfaces 3 (2011) 1015–1021.
[10] J. Lee, J. Bae, J. Heo, I.T. Han, S.N. Cha, D.K. Kim, M. Yang, H.S. Han, W.S. Jeon, J. Chung, J. Electrochem. Soc. 156 (2009) A905–A910.
[11] C. Martin, O. Crosnier, R. Retoux, D. Bélanger, D.M. Schleich, T. Brousse, Adv. Funct. Mater. 21 (2011) 3524–3530.
[12] W. Wang, R. Epur, P.N. Kumta, Electrochem. Commun. 13 (2011) 429–432.
[13] W. Wang, P.N. Kumta, ACS Nano 4 (2010) 2233–2241.
[14] L.F. Cui, L.B. Hu, J.W. Choi, Y. Cui, ACS Nano 4 (2010) 3671–3678.
[15] L. Hu, H. Wu, Y. Gao, A. Cao, H. Li, J. McDough, X. Xie, M. Zhou, Y. Cui, Adv. Energy Mater. 1 (2011) 523–527.
[16] M. Izu, T. Ellison, Sol. Energy Mater. Sol. Cells 78 (2003) 613–626.
[17] B.J. Landi, H.J. Ruf, C.M. Evans, C.D. Cress, R.P. Raffaelle, J. Phys. Chem. B 109 (2005) 9952–9965.
[18] B.J. Landi, C.D. Cress, C.M. Evans, R.P. Raffaelle, Chem. Mater. 17 (2005) 6819–6834.
[19] W.S. Rasband, ImageJ, U.S. National Institutes of Health. Bethesda, Maryland, USA 1997-2012, http://imagej.nih.gov/ij/.
[20] K. Evanoff, J. Benson, M. Schauer, I. Kovalenko, D. Lashmore, W.J. Ready, G. Yushin, ACS Nano 6 (2012) 9837–9845.
[21] G.Z. Yue, J.D. Lorentzen, J. Lin, D.X. Han, Q. Wang, Appl. Phys. Lett. 75 (1999) 492–494.
[22] A.T. Voutsas, M.K. Hatalis, J. Electrochem. Soc. 139 (1992) 2659–2665.
[23] P. Limthongkul, Y.-I. Jang, N.J. Dudney, Y.-M. Chiang, Acta Mater. 51 (2003) 1103–1113.
[24] R.A. Dileo, A. Castiglia, M.J. Ganter, R.E. Rogers, C.D. Cress, R.P. Raffaelle, B.J. Landi, ACS Nano 4 (2010) 6121–6131.
[25] T.D. Hatchard, J.R. Dahn, J. Electrochem. Soc. 151 (2004) A838–A842.
[26] J.P. Rong, C. Masarapu, J. Ni, Z.J. Zhang, B.Q. Wei, ACS Nano 4 (2010) 4683–4690.
[27] X.L. Li, J.H. Cho, N. Li, Y.Y. Zhang, D. Williams, S.A. Dayeh, S.T. Picraux, Adv. Energy Mater. 2 (2012) 87–93.
[28] S.L. Chou, Y. Zhao, J.Z. Wang, Z.X. Chen, H.K. Liu, S.X. Dou, J. Phys. Chem. C 114 (2010) 15862–15867.
[29] X.H. Liu, L. Zhong, S. Huang, S.X. Mao, T. Zhu, J.Y. Huang, ACS Nano 6 (2012) 1522–1531.
[30] H. Li, X. Huang, L. Chen, G. Zhou, Z. Zhang, D. Yu, Y. Jun Mo, N. Pei, Solid State Ionics 135 (2000) 181–191.